



# Surface enhanced substrate simulation optimized coupled PLS model for quantitative detection of acetone in transformer oil

Yihua Qian<sup>1</sup> · Qing Wang<sup>1</sup> · Siwei Pan<sup>1</sup> · Zhuang Yang<sup>2</sup> · Dingkun Yang<sup>3</sup>

Received: 22 August 2023 / Accepted: 28 December 2023 / Published online: 16 February 2024  
© The Author(s) 2024

## Abstract

Acetone is a reliable index to evaluate the aging state of oil paper insulation. It is of great significance to study a fast, highly sensitive and accurate method of detecting acetone in oil to ensure the safe and stable operation of oil-immersed transformers. In this paper, a method based on surface enhanced Raman spectroscopy for the detection of acetone in oil is investigated. Based on the mechanism of surface-enhanced Raman spectroscopy (SERS), a simulation model of surface-enhanced substrate was constructed using COMSOL software, and it was determined that the enhancement effect was better when silver nanowires/zinc oxide nanorods (Ag/ZnO) composite structure was selected. Ag/ZnO substrates were prepared by solvothermal method and experimentally tuned and characterized to obtain SERS substrates with high enhancement properties. The substrate coupled partial least square (PLS) model was used to establish a method for the detection of acetone in insulating oils, and its limit of quantification for acetone was 0.003 mg/g, which meets the requirements for engineering testing.

**Keywords** Surface enhanced Raman spectroscopy · Silver nanowires/zinc oxide nanorods · Oil · Acetone · PLS

## 1 Introduction

Oil-immersed power transformer is one of the core hub equipment of the power system [1]. The aging state of the oil-paper insulation is an important indicator for assessing the health of the transformer. Thus, accurate diagnosis of the aging state of a transformer is critical to the safe operation of a power system [2, 3].

The insulation system of oil-immersed power transformer is mainly composed of insulating oil and insulating paper [4]. In the process of long-term operation, the oil paper insulation material decomposes under the action of electric and thermal factors, producing a series of substances reflecting

operational faults and insulation aging characteristics [5, 6]. The content of acetone, as one of the aging characteristics of oil-paper insulation, can be used as a parameter to assess the aging condition of the insulation system [7]. Means of detection of dissolved acetone content in transformer oil mainly include high performance liquid chromatography (HPLC) [8], electrochemical method [9] and spectrophotometric method [10]. The most commonly used method is HPLC, but the complexity of the operation and the frequent replacement of columns determine that this method can only be completed in the laboratory and is not suitable for long-term monitoring [11]. Therefore, the development of an easy-to-operate, highly accurate and field-applicable method to detect the dissolved acetone content in insulating oils is of great value in enhancing the field analysis of oil-immersed transformer equipment.

Raman spectroscopy is a widely used spectroscopic technique to effectively detect and analyze the content of specific dissolved substances in liquid materials [12]. However, Raman spectroscopy has a weak scattering signal, which limits the accuracy and sensitivity in detecting trace substances [13]. SERS can effectively amplify the inherently weak Raman surface interface, and the Raman signals of molecules adsorbed on the surface of rough metal nanostructures can be amplified by  $10\text{--}10^9$  times, which can

✉ Yihua Qian  
595295424@qq.com

Zhuang Yang  
zyoung@cqu.edu.cn

<sup>1</sup> Electric Power Research Institute of Guangdong Power Grid Corporation, Guangzhou 510080, China

<sup>2</sup> School of Electrical Engineering, Chongqing University, Chongqing 400044, China

<sup>3</sup> School of Advanced Manufacturing Engineering, Chongqing University of Posts and Telecommunications, Chongqing 400065, China

effectively solve the problem of insufficient signals in the detection of trace substances [14]. The SERS technique allows for rapid quantitative prediction by acquiring spectral information about the analyte. Zhu et al. [15] applied gold and silver core–shell nanoflowers (Au@Ag NFs) as SERS active substrates to predict 2,4-D and imidacloprid in milk in the range of  $1.0 \times 10^{-3}$  to  $1.0 \times 10^2$  ng/mL. Jiao et al. [16] prepared silver nanoparticles coated with zinc oxide nanoflowers (Ag@ZnO NFs) as a SERS substrate and combined it with a chemometric method for the quantitative detection of deltamethrin in wheat with a detection limit of  $0.16 \mu\text{g}\cdot\text{kg}^{-1}$ .

In this study, combined with simulation guidance, Ag/ZnO SERS substrates were first prepared by in situ modification of ZnO on Ag nanomaterials by chemical reduction. Then, a high sensitivity and high accuracy method for the determination of dissolved acetone in transformer oil was established based on PLS model. The method is applicable to the rapid and accurate determination of acetone content in oil-paper insulated electrical equipment, which can monitor the safety and stability of the power system in time.

## 2 Materials and methods

### 2.1 Materials

The details of the materials used in this paper are shown in Table 1.

### 2.2 Surface enhanced substrate simulation design

In the application of SERS, it is very important to choose a suitable substrate because the composition, size, shape and other parameters of the SERS substrate will directly affect the SERS signal enhancement effect. Therefore, it is first necessary to simulate and analyze the electromagnetic enhancement performance of the surface-enhanced substrate based on the mechanism of SERS and using the COMSOL multiphysics field simulation software on the computer. Its 3-dimensional model is shown in Fig. 1a. Finally, the

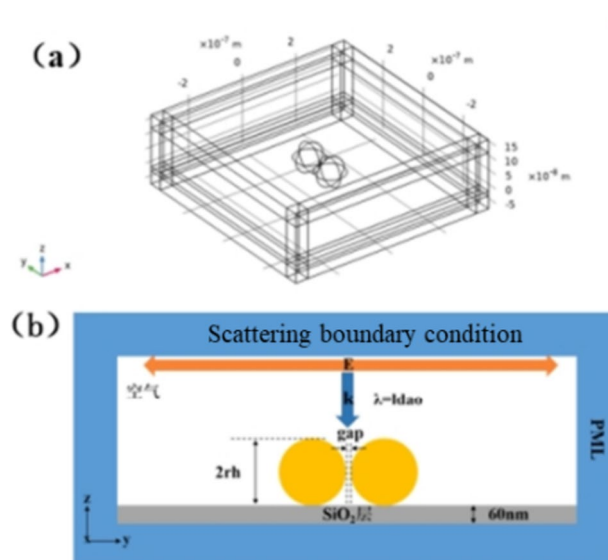


**Fig. 1** a 3D simulation model diagrams and b 2D configurations of surface-enhanced substrates

optimal parameters were determined to provide guidance for the preparation of materials for later experiments, while saving experimental costs and time. This simulation method is helping to understand the effects of various parameters on EM enhancement and guiding the subsequent preparation of highly SERS-active substrates. Figure 1b demonstrates the 2-dimensional configuration of the Ag/ZnO composite surface-enhanced substrate.

### 2.3 Apparatus

In this paper, high-resolution transmission electron microscopy (HRTEM) and selected-area electron diffraction (SAED) will be performed on a transmission electron microscope (Tecnai G2 F30, FEI, USA). Samples were prepared by placing a drop of sample solution on a porous carbon film supported by a copper grid and dried naturally, and imaged at an accelerating voltage of 200 kV. In this work, all Raman spectroscopy experiments were performed based

**Table 1** Chemical reagents and materials required for the experiment

Materials	Molecular formula	Clarification
Silver nanowire-ethanol suspension	CST-NW-S30	10 mg/L
1,4-Benzenedithiol (BDT)	$\text{C}_6\text{H}_6\text{S}_2$	>98%
Rhodamine 6G (R6G)	$\text{C}_{28}\text{H}_{31}\text{N}_2\text{O}_3\text{Cl}$	≥95%
Zinc chloride	$\text{ZnCl}_2$	>99.99%
N,N-dimethylformamide (DMF)	$\text{HCON}(\text{CH}_3)_2$	>99.5%
Dimethylsiloxane	$[-\text{Si}(\text{CH}_3)_2\text{O}-]_n$	For oil bath heating
Pure water	$\text{H}_2\text{O}$	–
Anhydrous ethanol	$\text{C}_2\text{H}_6\text{O}$	>95%

on an integrated detection platform for confocal laser Raman spectroscopy built by our group. The platform includes laser, optical microscope, filters, Raman spectrometer, a CCD detector, etc., as described in detail in [17].

In addition, a liquid–liquid extraction method was used and pure water was selected as the extractant, and an extraction ratio of 20:1 was chosen for the enrichment of acetone. Pure water is chemically relatively stable, and its Raman scattering is weak and does not interfere with fluorescence in the measurement range of Raman spectroscopy [18].

## 2.4 SERS detection

The SERS test procedure for acetone in insulating oil is as follows.

- (1) Liquid–liquid extraction. Using pure water as the extractant, the standard liquid, which is insulating oil with acetone dissolved in it, was mixed thoroughly with the extractant, and the lower acetone extract was taken and passed into a quartz band-tube cuvette.
- (2) Placement of substrate and acetone extracts. Place the prepared substrate in the sample cell so that the acetone extraction solution is in full contact with the substrate.
- (3) Spectrum correction. The Raman peak at  $520.7 \text{ cm}^{-1}$  of the silicon wafer was used as a reference for the calibration spectra.
- (4) Selection of detection point. The spatial position of the sample stage is adjusted by a 3D fine-tuning stage and combined with a color CMOS monitoring camera to ensure that the laser is focused on the SERS substrate and the final SERS detection point is selected.
- (5) Setting parameters. A  $50\times$  telephoto objective and a 1200 line/750 nm grating were used. Laser powers of 70 and 50 mW were selected for the detection of R6G molecules and acetone molecules, respectively. For the detection of R6G molecular probes, the integration time was set to 0.1 s and the cumulative number of integrations was 10. For the acetone molecule, the number of accumulated integrations was chosen to be 100 due to its weak signal strength.
- (6) Spectral analysis. First, the raw spectral data are pre-processed to improve the data quality. Then, the Raman spectral data were qualitative and quantitative analyses.

## 2.5 PLS model

PLS is a multivariate data statistical analysis method for solving regression problems with multiple independent variables and one or more dependent variables [19, 20]. In this way, PLS can reduce the correlation between variables and improve the accuracy and stability of the regression model while retaining most of the original variable information.

Calibration correlation coefficient  $R_c$  and prediction correlation coefficient  $R_p$  can be used to evaluate the fitting effect of PLS model. The closer  $R_c$  and  $R_p$  are to 1, the better the model fits the sample data. In addition, in order to evaluate the predictive ability of the PLS model, metrics such as corrected root mean square error (RMSECV), root mean square error of prediction (RMSEP), and MAPE are used. The formulas for RMSECV and RMSEP are as follows.

$$\text{RMSECV} = \sqrt{\frac{\sum_{i=1}^c (\hat{y}_i - y_i)^2}{c}} \quad (1)$$

$$\text{RMSEP} = \sqrt{\frac{\sum_{i=1}^p (\hat{y}_i - y_i)^2}{p}} \quad (2)$$

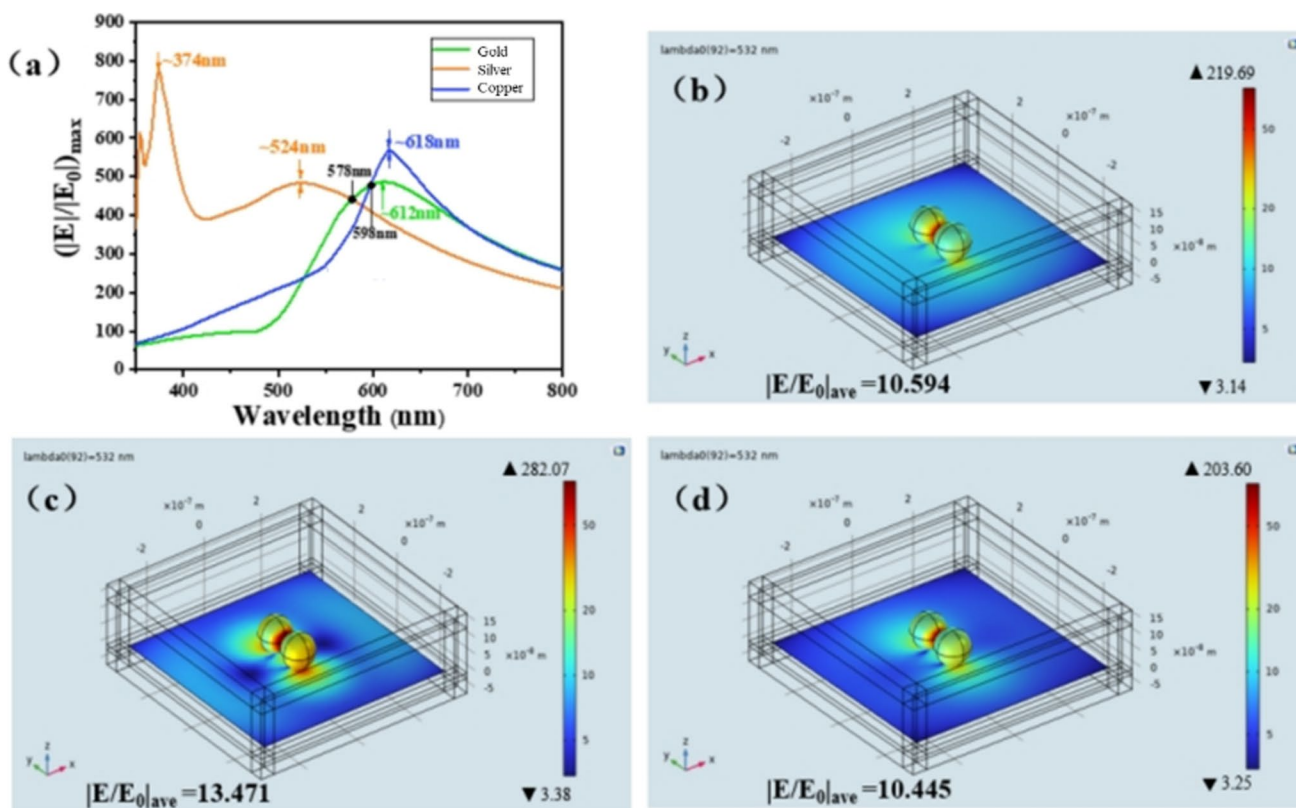
where  $c$  is the number of samples in the calibration set,  $y_i$  is the standard concentration of sample  $i$  in the standard series,  $\hat{y}_i$  is the estimated concentration of sample  $i$  in the standard series.

## 3 Results and discussion

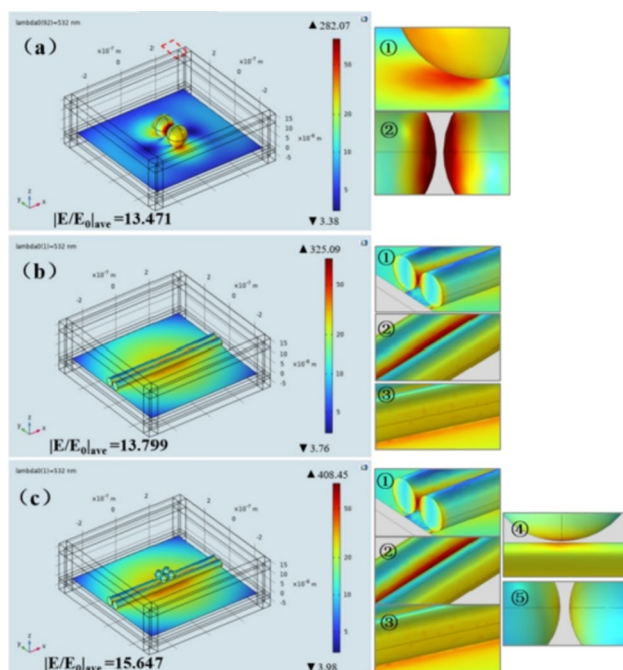
### 3.1 Selection of nanomaterials and morphology

Figure 2a shows the simulation results of the relationship between the maximum surface electric field enhancement  $|E/E_0|_{\max}$  and the excitation wavelength  $\lambda$  of the nanosphere dimer of gold, silver and copper materials. As can be seen from the figure, silver has a better electric field enhancement compared to gold and copper. The wavelength in the actual Raman spectroscopy test is 532 nm. Figure 2b–d shows the surface electric field distribution of Au, Ag and Cu materials at the wavelength of 532 nm, respectively. The maximum electric field enhancement multiples  $|E/E_0|_{\max}$  are 219.69, 282.07, and 203.6 for gold, silver, and copper materials, respectively, and the average electric field enhancement sizes  $|E/E_0|_{\text{ave}}$  are 10.594, 13.471, and 10.445, respectively. It can be seen that at a wavelength of 532 nm, the silver material usually has a higher SERS enhancement with more hot-spot distribution and greater strength.

Figure 3 illustrates the electric field distribution of nanodimers with different structures. As can be seen in Fig. 3a, the hot spots of silver nanosphere dimers exist in the double-sphere gap (①) and between the sphere and the substrate (②). From Fig. 3b, it can be seen that the hotspots of the silver nanowire dimer exist at the ends of the silver nanowire structure (①), in the gap between the two silver nanowires (②), and in the region where the silver nanowires are connected to the underlying substrate (③). From Fig. 3b, it can



**Fig. 2** a The relationship between the particle size of dimers with different shapes and the electric field enhancement characteristics (excitation wavelength is 532 nm, gap is 5 nm). Electric field distribution of nanosphere dimers of **b** gold, **c** silver, and **d** copper



**Fig. 3** Electric field distribution of **a** silver nanospheres, **b** silver nanowires, **c** silver nanowires/zinc oxide nanocomposite (on the right is the enlarged view of SERS hotspot area)

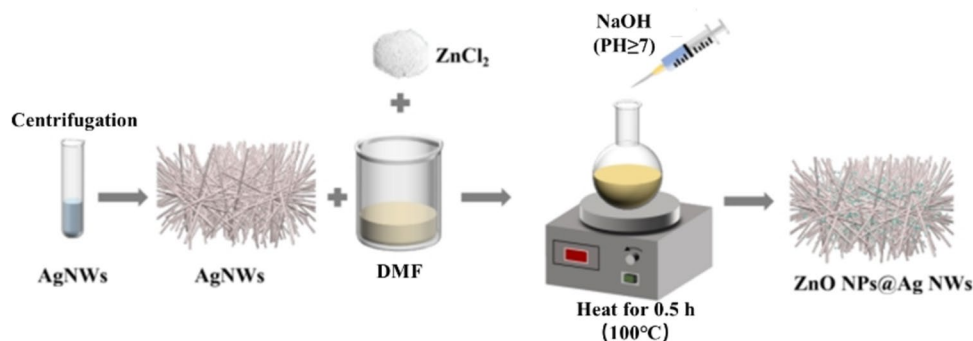
be seen that the “hot spots” mainly exist in two aspects. On the one hand, the hot spots at the top of the silver nanowire structure (①), in the gap between two silver nanowires (②), and between the silver nanowire and the underlying silver film (③) originate from the silver nanowire structure itself. On the other hand, new hotspots with higher hotspot intensities appear in the gap between the silver nanowire and the ZnO NPs (④) as well as in the gap between two ZnO NPs (⑤). The silver nanowire composite structure has the highest SERS enhancement ability, so the silver nanowire/zinc oxide nanorods composite structure was chosen for Raman enhancement in this paper.

### 3.2 Substrate performance optimization

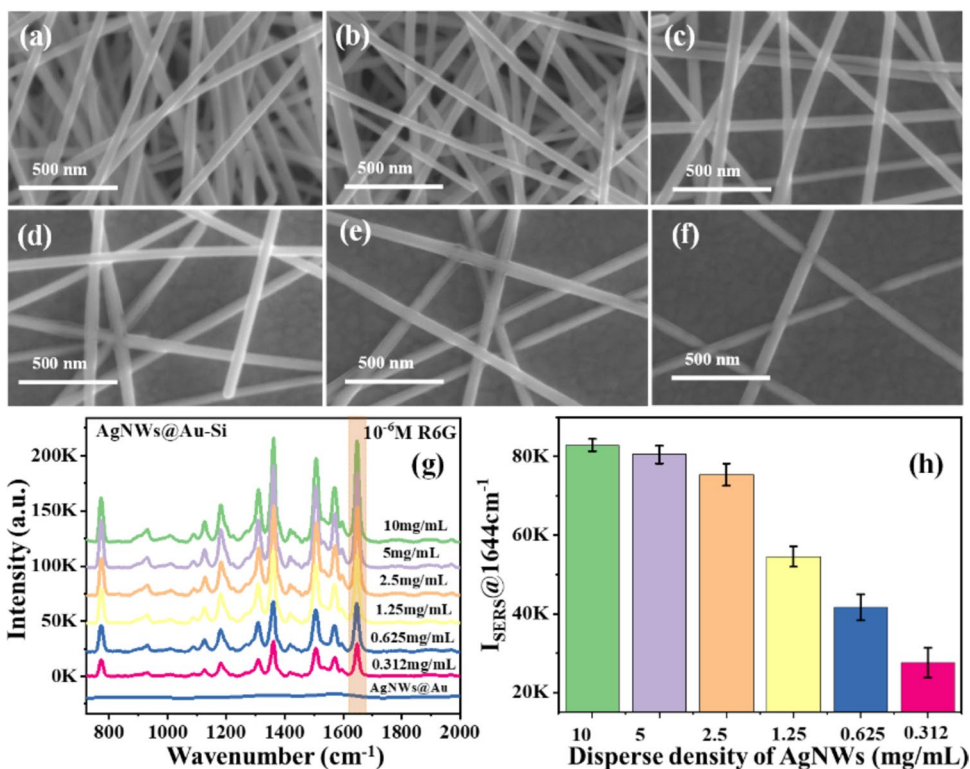
According to the simulation results, silver nanowire/zinc oxide nanorods (Ag/ZnO) composite structure is selected for the SERS substrate in this paper. Ag/ZnO composite SERS substrates were experimentally prepared and optimally tuned for practical enhancement. The preparation process is shown in Fig. 4.

Figure 5a–f demonstrates the SEM images of Ag NWs self-assembled substrates with different Ag NWs dosages (dispersion densities from 10 to 0.312 mg/mL). As the

**Fig. 4** Preparation process of ZnO particles compounded on Ag NWs



**Fig. 5** SEM images of Ag NWs substrates with different dosages: **a** 10 mg/mL, **b** 5 mg/mL, **c** 2.5 mg/mL, **d** 1.25 mg/mL, **e** 0.625 mg/mL, **f** 0.312 mg/mL; **g** all adsorbed  $10^{-6}$  M R6G with different SERS spectra of Ag NWs substrates of with different amounts; **h** comparison of the intensity of the corresponding characteristic peaks at  $1649\text{ cm}^{-1}$



density of the Ag NWs dispersion decreases, the formed reticulation gradually decreases and the formed 3D structure is gradually sparse. Figure 5g shows the Raman spectra of self-assembled substrates of Ag NWs and SERS spectra of Ag NWs with different dispersion densities adsorbed with  $10^{-6}$  M R6G. Figure 5h shows that the average SERS signal intensity at  $1644\text{ cm}^{-1}$  shows a decreasing trend as the dispersion density of Ag NWs decreases. Considering the cost and SERS sensitivity, the SERS substrate with Ag NWs dispersion density of 2.5 mg/mL was selected for subsequent experiments.

### 3.3 Ag/ZnO substrate characterization

The elements and morphology of the prepared Ag/ZnO composites were characterized using transmission electron

microscopy. As can be seen from the TEM image (Fig. 6a), the Ag NWs in the Ag/ZnO composites still maintain the original cross-network morphology, forming a dense porous structure. The modified ZnO NPs are mostly loaded with small particles and uniformly anchored on the surface of Ag NWs, which are mainly distributed at the edges and porous structures of Ag NWs. As a result, the Ag NWs generated LSPR and the electron transfer interface of Ag NWs/ZnO was formed. As can be seen from the EDS plot in Fig. 6b, except for the peaks of Ag, Zn, O, and Cu, and there are no other obvious miscellaneous peaks. The peak assigned Cu is generated by the copper mesh, indicating that no other impurities are present in the prepared Ag/ZnO composites. From the SEM image of Fig. 6c, it can be seen that the ZnO NPs are distributed on the Ag surface.

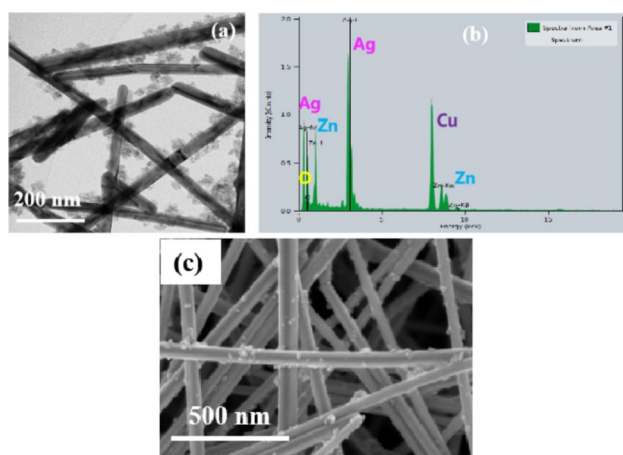


**Fig. 6** Characterization of Ag/ZnO by transmission electron microscopy: **a** TEM; **b** EDS spectrum **c** SEM

### 3.4 Sensitivity of the substrate

The enhancement factor is an important metric to quantify the performance of the substrate SERS. The commonly used enhancement factor during practical feature detection is calculated by Eq. (3):

$$EF_{\text{SERS}}(\omega_\nu) = \frac{I_{\text{SERS}}/N_{\text{SERS}}}{I_{\text{out}}/N_{\text{out}}} \quad (3)$$

where  $I_{\text{SERS}}$  and  $N_{\text{SERS}}$  represent the signal intensity of Raman spectra of surface-enhanced target molecules and the number of molecules contained within the signal region;  $I_{\text{out}}$  and  $N_{\text{out}}$  represent the signal intensity of ordinary Raman signals of target molecules and the number of molecules contained within the signal region.

Figure 7 demonstrates the SERS spectrum of  $10^{-12}$  M R6G versus the  $10^{-6}$  M R6G normal Raman spectrum where the peak at  $1649 \text{ cm}^{-1}$  was selected as the characteristic peak for the enhancement factor calculation. The SERS detection intensity  $I_{\text{SERS}}$  of  $10^{-12}$  M R6G adsorbed on ZnO NPs@Ag NWs substrate was about 528.498, while the ordinary Raman detection intensity  $I_{\text{out}}$  of  $10^{-6}$  M R6G was about 12.558. Since the SERS detection and the ordinary Raman detection use the same measurement and preparation conditions, they therefore have similar detection volumes and molecular absorption surface areas. Therefore,  $N_{\text{SERS}}$  and  $N_{\text{out}}$  are mainly determined by the concentration of R6G, i.e.,  $N_{\text{SERS}}/N_{\text{out}} = C_{\text{SERS}}/C_{\text{out}} = 10^6$ . This gives an enhancement factor of about  $4.21 \times 10^7$  for the ZnO NPs@Ag NWs substrate. The same method was used to calculate the enhancement factor of pure Ag NWs, which was obtained to be about  $9.8 \times 10^6$ . Compared with the pure Ag NWs, the SERS enhancement performance of the ZnO NPs@Ag NWs composite substrate is improved by a factor of 4.3, which

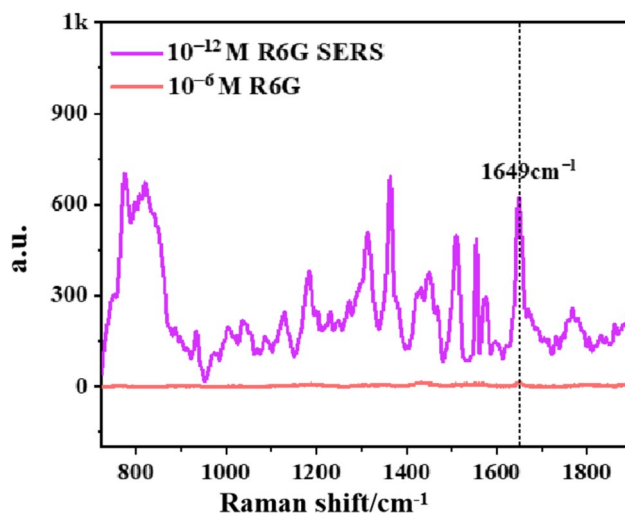


**Fig. 7** SERS spectra of  $10^{-12}$  M R6G adsorbed on ZnO NPs@Ag NWs and ordinary Raman spectra of  $10^{-6}$  M R6G

again suggests that the introduction of ZnO NPs improves the effective charge transfer effect in the metal-semiconductor-molecule system and thus enhances the SERS activity of the composite substrate.

### 3.5 Simulation and analysis of Raman spectra of acetone

Prior to Raman testing of trace amounts of acetone, the Raman peaks of acetone need to be identified. The Raman vibrational properties of the acetone molecule were simulated and analyzed using Gaussian09W software, and the vibrational attributions of the main Raman signals were pointed out. Among the Raman spectral peaks of pure acetone,  $786$ ,  $1069$ ,  $1219$ ,  $1428$ ,  $1707$  and,  $2923 \text{ cm}^{-1}$  were more pronounced, which corresponded to  $769$ ,  $1037$ ,  $1193$ ,  $1394$ ,  $1719$ , and  $2934 \text{ cm}^{-1}$  of the simulation model, respectively (Fig. 8).

Figure 9 compares the Raman spectra of a transformer oil solution, a transformer oil solution with a high concentration of acetone dissolved in it, pure acetone, and an extracted solution with a high concentration of acetone. From the figure, it can be seen that the spectral information in the transformer oil is extremely complex, and most of the Raman peaks of acetone (e.g.,  $1069$ ,  $1219$ ,  $1428$ , and  $2923 \text{ cm}^{-1}$ ) are covered by the complex background Raman peaks of the transformer oil itself, and in particular, the spectral peak at  $2923 \text{ cm}^{-1}$ , which is the strongest signal of the Raman of acetone, is completely submerged. This is due to the extreme complexity of the substances in the transformer oil, which seriously affects the Raman spectroscopic detection of acetone. The interference of other stray peaks in the transformer

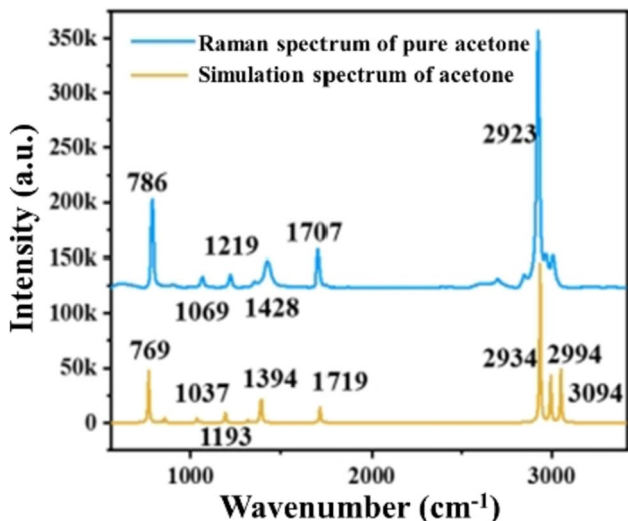


Fig. 8 Raman spectra and simulation plots of acetone

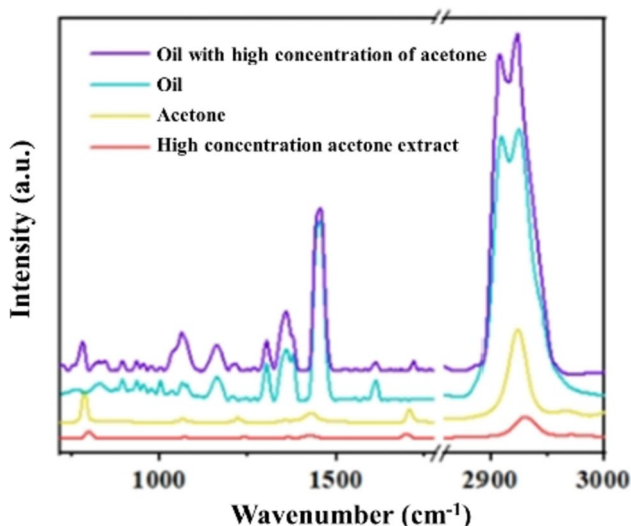


Fig. 9 Raman spectra of different solutions

oil can be effectively reduced by utilizing the method of liquid–liquid extraction.

As shown in Fig. 10, under the same test conditions, (a) surface-enhanced Raman spectroscopy based on Ag/ZnO substrate and (b) ordinary Raman spectroscopy were performed on 7.29 mg/g acetone extract, respectively, and compared with (c) Raman spectra of pure acetone, (d) Raman spectra of pure water, and (e) Raman spectra of Ag/ZnO substrate at the same time. Combined with the Raman spectrum of the pure acetone molecule, the peak 800  $\text{cm}^{-1}$  was identified as originating from the C–C bond stretching vibration in the acetone molecule. The Raman signal at 1074  $\text{cm}^{-1}$  is caused by C–C shear motion and C–H wobble in the acetone

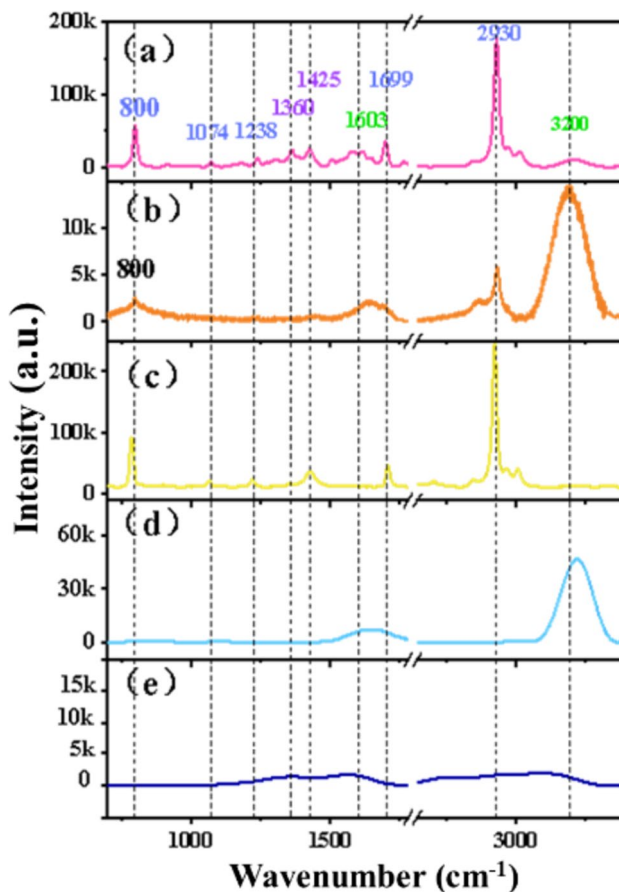


Fig. 10 Raman spectroscopy (a) surface-enhanced Raman spectroscopic detection based on Ag/ZnO substrate, (b) normal Raman spectroscopic detection, (c) Raman spectroscopy of pure acetone, (d) Raman spectroscopy of pure water and (e) Raman spectroscopy of Ag/ZnO substrate)

molecule. The Raman signal at 1238  $\text{cm}^{-1}$  is attributed to C–C shear motion as well as C–H shear motion. The Raman peak at 1699  $\text{cm}^{-1}$  originates from C=O stretching in the acetone molecule. The Raman peak at 2930  $\text{cm}^{-1}$  is caused by C–H stretching.

Among the five acetone-enhanced Raman signals, the Raman peak at 2930  $\text{cm}^{-1}$  is the strongest. Therefore, 2930  $\text{cm}^{-1}$  was selected as the characteristic peak of the dissolved acetone molecules in the transformer oil extract in the surface-enhanced Raman spectroscopy detection, and was used for further analysis.

### 3.6 Quantitative detection of acetone in oil based on PLS

In order to determine the surface enhancement properties of the prepared ZnO NPs@Ag NWs composite SERS substrate for use in different concentrations of acetone extracts, SERS was performed on configured acetone standard gradient

extracts in this paper. The measured spectral data were baseline corrected using LabSpec Raman data analysis software. Then, the Savitzky-Golay module in Origin software was utilized for smoothing noise reduction. Finally, the Raman peak at  $3200\text{ cm}^{-1}$  of pure water was used as the internal standard peak for normalization, and the SERS spectrum of the pre-treated acetone standard gradient extract is shown in Fig. 11.

Raman spectral data for SERS detection of acetone standard gradient extracts were obtained using the above experiments. The  $2930\text{ cm}^{-1}$  Raman peak was used as the target characteristic peak for SERS detection of acetone. Gaussian fitting of the target characteristic curve for each sample was performed using Origin software to obtain the Raman intensity of the target characteristic peak at  $2930\text{ cm}^{-1}$ . The mathematical regression relationship between the characteristic peak intensity of acetone and the acetone content in the corresponding insulating oil was established using the acetone content as the independent variable and the characteristic peak intensity as the dependent variable. In order to better present the results, the horizontal coordinates were logarithmized and the results of the regression built based on the least squares method are shown in Fig. 12.

The linear regression equation established is shown in Fig. 12. Where  $x$  is the concentration of acetone in oil;  $y$  is the Raman intensity corresponding to the target characteristic peak at  $2930\text{ cm}^{-1}$ .

The linear regression equation established is:

$$y = 18860.701x + 2857.784 \quad (4.1)$$

where  $x$  is the concentration of acetone in the corresponding insulating oil;  $y$  is the Raman intensity of the target characteristic peak at  $2930\text{ cm}^{-1}$  correspondingly.

In the measured range, there is a good linear relationship between the intensity of the characteristic peak of acetone and the content of acetone in the corresponding insulating oil, and the goodness of fit is 0.984. The average peak intensity of the noise signal is about 989.240 a.u. Considering

the triple signal-to-noise ratio, the lower limit of detection of acetone is calculated to be  $0.00583\text{ mg/g}$ , which meets the demand of practical engineering testing in the field of power industry.

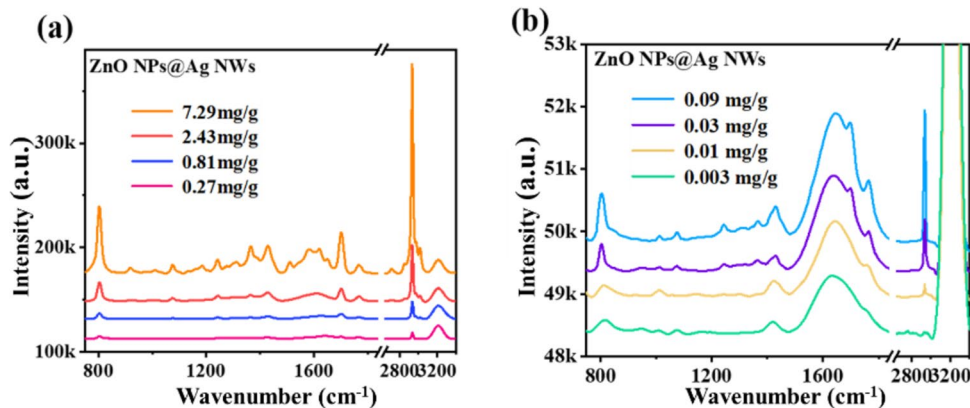
The results showed that the quantitative model did not fit well in the lower concentration range. This is because the linear regression model uses only one Eigenpeak and ignores information in multi-featured peaks and even in the full spectrum.

In this paper, a PLS model was used to establish a statistical relationship between acetone content and full-spectrum intensity. The 32 samples from 48 standard acetone extracts were used as the training set and 16 samples as the prediction set. The SERS spectra and acetone concentration matrix of the acetone extracts were imported into Unscrambler X multivariate data analysis software for PLS regression analysis. The model performed well in the calibration set with  $R_c = 0.992$  and  $RMSECV = 0.215\text{ mg/g}$ . The model performed well in the test set with  $R_c = 0.981$  and  $RMSECV = 0.328\text{ mg/g}$ . The results show that the predictive stability of the PLS model is better than that of the linear quantitative model. The PLS model was chosen as the quantitative analysis method for acetone extraction SERS, and its limit of quantification (LOQ) for acetone was  $0.003\text{ mg/g}$ , which meets the requirements of engineering testing.

## 4 Conclusion

In this paper, combined with the developed Ag/ZnO composite substrate, based on the integrated detection platform and extraction technology, SERS detection of acetone in insulating oil was performed. Firstly, the electric field distribution of the surface-enhanced substrate is investigated by simulation to provide some basis and guidance for the subsequent preparation of the surface-enhanced substrate. Then, Ag/ZnO composite SERS substrates were prepared using solvothermal and self-assembly methods, and experimentally tuned and characterized in various ways in order

**Fig. 11** SERS detection spectrum of acetone standard gradient extracts based on surface enhancement of ZnO NPs@Ag NWs: **a** 7.29–0.27 mg/g; **b** 0.09–0.003 mg/g





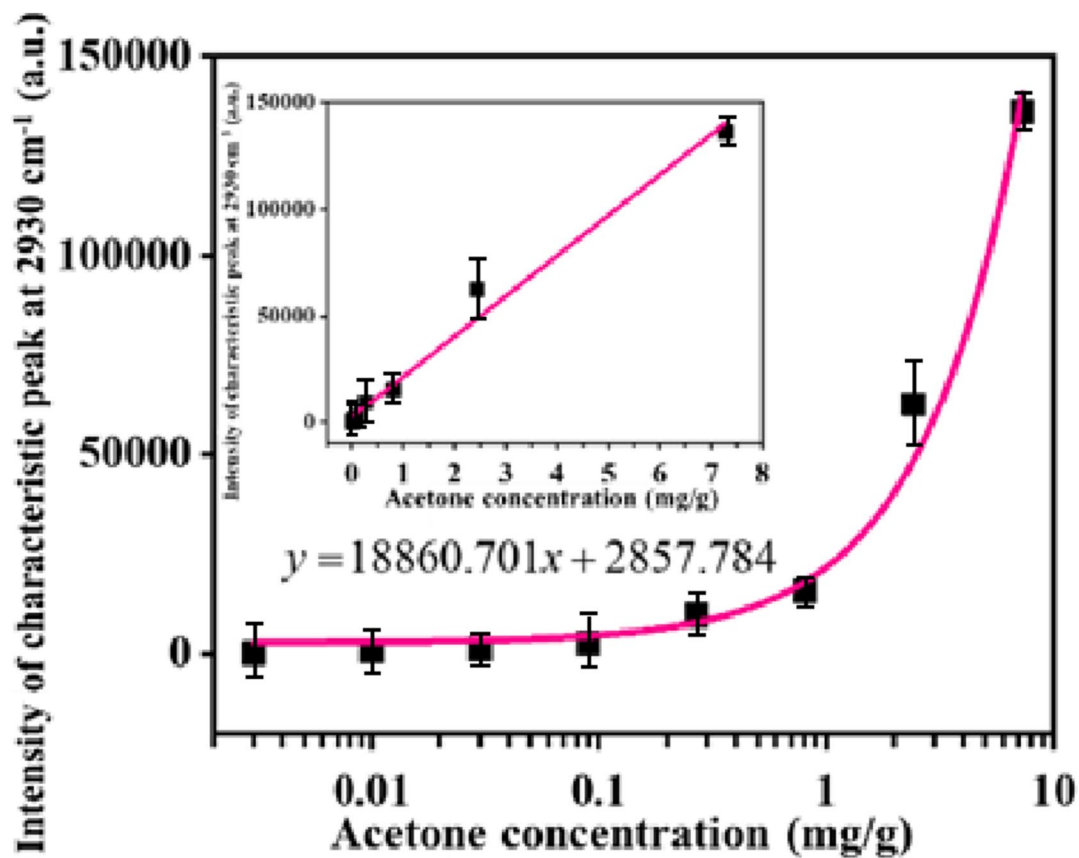


**Fig. 12** Relationship between acetone concentration and intensity of the characteristic peak at  $2930\text{ cm}^{-1}$  with non-linear horizontal coordinates (plots of the corresponding linear horizontal coordinates are shown in the inset)

to obtain SERS substrates with high enhancement properties. Finally, the substrate was used for the SERS detection of dissolved trace acetone in insulating oils, and a SERS-coupled PLS quantitative detection method for acetone in insulating oils was established, with a limit of quantification of  $0.003\text{ mg/g}$  for acetone, which meets the requirements of engineering detection.

**Acknowledgements** We gratefully acknowledge the research grants provided by China Southern Power Grid Co., Ltd. Science and Technology Project Fund (No. GDKJXM20210087).

## Declarations

**Conflict of Interest** The authors declare no potential conflict of interests.

**Open Access** This article is licensed under a Creative Commons Attribution 4.0 International License, which permits use, sharing, adaptation, distribution and reproduction in any medium or format, as long as you give appropriate credit to the original author(s) and the source, provide a link to the Creative Commons licence, and indicate if changes were made. The images or other third party material in this article are included in the article's Creative Commons licence, unless indicated otherwise in a credit line to the material. If material is not included in the article's Creative Commons licence and your intended use is not

permitted by statutory regulation or exceeds the permitted use, you will need to obtain permission directly from the copyright holder. To view a copy of this licence, visit <http://creativecommons.org/licenses/by/4.0/>.

## References

1. Shu, Y.: Research and application of UHV power transmission in China. *IET High Voltage*. **3**(1), 1–13 (2018)
2. Liao, R.J.: The effects of insulating oil replacement upon power transformer condition assessment. *Electr. Power Compon. Syst.* **43**(17), 1971–1979 (2015)
3. Wang, Y.Y.: Investigation of characteristic parameters for condition evaluation of transformer oil-paper insulation using frequency domain spectroscopy. *Int. Trans. Electr. Energy Syst.* **25**(11), 2921–2932 (2015)
4. Saha, T.K.: Review of modern diagnostic techniques for assessing insulation condition in aged transformers. *IEEE Trans. Dielectr. Electr. Insul.* **10**(5), 903–917 (2003)
5. Martin, D.: An updated model to determine the life remaining of transformer insulation. *IEEE Trans. Power Deliv.* **30**(1), 395–402 (2015)
6. Liu, X.: Study on influences and elimination of test temperature on PDC characteristic spectroscopy of oil-paper insulation system. *J. Electr. Eng. Technol.* **10**(3), 1107–1113 (2015)

7. Gu, Z.: Application of Raman spectroscopy for the detection of acetone dissolved in transformer oil. *J. Appl. Spectrosc.* **85**(2), 225–231 (2018)
8. Kalkan, E.A.: Quantitative clinical diagnostic analysis of acetone in human blood by HPLC: a metabolomic search for acetone as indicator. *J. Anal. Methods Chem.* **2016** (2016)
9. Zhou, Q.: Fabrication and characterization of highly sensitive acetone chemical sensor based on ZnO nanoballs. *Materials* **10**(7), 799 (2017)
10. Berntsson, S.: Spectrophotometric determination of acetone by the salicylaldehyde method. *Anal. Chem.* **28**(8), 1337–1337 (1956)
11. Kolb, B.K.: Proof of bacteria and the activity of chemical and natural antibiotics by headspace gas chromatography. *J. Anal. Sci. Technol.* **10**(1), 9 (2019)
12. Yang, Z.: A novel recognition method of aging stage of transformer oil-paper insulation using Raman spectroscopic recurrence plots. *IEEE Trans. Dielectr. Electr. Insul.* **29**(3), 1152–1159 (2022)
13. Liu, B.: Detection of pesticides in fruits by surface-enhanced Raman spectroscopy coupled with gold nanostructures. *Food Bioprocess Technol.* **6**, 710–718 (2013)
14. Wang, K.: Shell thickness-dependent Au@Ag nanoparticles aggregates for high-performance SERS applications. *Talanta* **195**, 506–515 (2019)
15. Zhu, A.F.: Au@Ag nanoflowers based SERS coupled chemometric algorithms for determination of organochlorine pesticides in milk. *Lwt Food Sci. Technol.* **150**, 111978 (2021)
16. Jiao, T.H.: Quantification of deltamethrin residues in wheat by Ag@ZnO NFs-based surface-enhanced Raman spectroscopy coupling chemometric models. *Food Chem.* **337**, 127652 (2021)
17. Wan, F.: Charge transfer effect on Raman and surface enhanced Raman spectroscopy of furfural molecules. *Food Chem.* **7**(8), 210 (2017)
18. Zhang, L.J.: Microdroplet extraction assisted ultrasensitive Raman detection in complex oil. *Lab Chip* **21**(11), 2217–2222 (2021)
19. Li, H.H.: Simultaneous quantification of deoxymyoglobin and oxymyoglobin in pork by Raman spectroscopy coupled with multivariate calibration. *Food Chem.* **372**, 131146 (2022)
20. Du, Y.W.: Diagnosis of hyperthyroidism and hypothyroidism serum by SVM-based Raman spectroscopy. *Laser Phys. Lett.* **16**(6), 065602 (2019)

**Publisher's Note** Springer Nature remains neutral with regard to jurisdictional claims in published maps and institutional affiliations.